Iranian Journal of Medical Physics

ijmp.mums.ac.ir

Determination of Radiation Shielding Features of Polyvinyl Alcohol/Magnetite-Bismuth Oxide Composite Using Precise Computational Methods and Monte Carlo Code

Fariba Baroonzadeh[1], Maziyar Mahdavi[1,2*], Mohammad Amin Hosseini[2,3], Reza Jalli[4]

1. Department of Radiology, School of Paramedical Sciences, Shiraz University of Medical Sciences, Shiraz, Iran.
2. Ionizing and Non-Ionizing Radiation Protection Research Center (INIRPRC), School of Paramedical Sciences, Shiraz University of Medical Sciences, Shiraz, Iran.
3. Physics Department, Università degli Studi di Torino, Turin, Italy.
4. Department of Radiology, Medical Imaging Research Center, Shiraz University of Medical Sciences, Shiraz, Iran

ARTICLE INFO

Article type:
Original Paper

Article history:
Received: July 24, 2023
Accepted: Nov 05, 2023

Keywords:
Polyvinyl Alcohol
Magnetite
Bismuth Oxide
Shield
Computed Tomography (CT)
MCNP Code

ABSTRACT

Introduction: Bismuth efficiency in shielding superficial tissues in computed tomography (CT) scans has been challenged due to the imbalance between image quality and dose reduction. The aim of this study is to reduce bismuth in shields and investigate the possibility of substitution with lower atomic materials.

Material and Methods: Five different compounds, including raw polyvinyl alcohol (PVA) and four other samples containing variable weight fractions of bismuth oxide and with a constant fraction of magnetite were selected. Shielding factors, including linear attenuation coefficient(μ), mass attenuation coefficient(μ_ρ), half-value layer (HVL), electron density (N_e), and effective atomic number (Z_{eff}), were evaluated over a wide range of energy by precise computational methods, XCOM, and Monte Carlo N-Particle code.

Results: Increasing the bismuth oxide concentration improves the radiation attenuation and absorption process. This effect was observed in the μ_ρ graphs to medium energies (E < 0.3560 MeV).The simultaneous evaluation of N_e and Z_{eff} predicts increased absorption due to the increased and dominant photoelectric effect (<0.1000 MeV), the raised Compton effect (0.1000 < E < 0.3560 MeV; followed by scattering owing to the predominant Compton effect), and formation (E ≈ 1.2200 MeV)and dominance of pair production phenomenon (E > 3.0000 MeV).Also, a quantitative analysis of absorption through HVL in several used energies showed the efficacy of these compounds in ionizing radiation absorption.

Conclusion: This study establishes the advantages of substituting bismuth with compounds having lower atomic number materials, and the possibility of alleviating bismuth and replacing it with magnetite and PVA in designing radiation shields in CT scans has been confirmed.

►*Please cite this article as:*
Baroonzadeh F, Mahdavi M, Hosseini MA, Jalli R. Determination of Radiation Shielding Features of Polyvinyl Alcohol/Magnetite-Bismuth Oxide Composite Using Precise Computational Methods and Monte Carlo Code. Iran J Med Phys 2024; 21: 381-390.10.22038/ijmp.2023.73865.2311.

Introduction

Ionizing radiations (including X-rays and gamma-rays), despite their widespread and unique usages in various industries, can be harmful to the environment, especially to human health, and cause damage at the cellular level and throughout the whole body [1]. Therefore, to reduce the risks of these problems, three principles of reducing time, increasing distance, and using radiation-absorbing materials should be applied as much as possible [1-2].

Polymer composites have been introduced as a new solution to construct radiation-absorbing materials. Since they utilize polymers (so-called matrices) in their structure and fillers for loading into matrices [3-4], considering a variety of polymers and choosing suitable fillers, they can represent a desirable efficiency against ionizing radiations. Concerns about traditional materials, such as bulk lead in the construction of radiation-absorbing materials, have been raised for a long time, such as high toxicity, fragility, and high weight of products. Therefore, it is expected that through an approach to polymer composites, besides achieving the desired efficiency in radiation absorption and attenuation, many of the hazards posed by traditional materials will also be eliminated [3].

Extensive efforts have been made to reduce and substitute lead (Z = 82), including using high-atomic materials such as bismuth (Z = 83) and tungsten (Z = 74) in the design of polymer composites with the ability to absorb radiation [5-9]. Recent studies have also shown the more desirable radiation shielding efficiency of the mentioned fillers in smaller sizes [7-9].

However, newer challenges to absorbing materials containing elements with high atomic numbers seem

*Corresponding Author: Tel: +98-7132289113; Fax: +98-7132289113; Email: mahdavi@sums.ac.ir

to show off. Computed tomography (CT) scans, which account for the largest share of medical radiation exposure [10-11], have been the subject of extensive studies on radiation dose estimation to patients [12-16]. To reduce patient exposure, absorbing materials such as bismuth have been used to shield superficial tissues [17]. However, a key challenge remains in achieving an optimal balance between dose reduction and preserving image quality [18].Numerous studies have confirmed that using bismuth-containing shields can lead to a detrimental reduction of clinical image quality by creating artifacts [17, 19-21]. The secondary radiation produced by materials with high atomic numbers during radiation collisions can be considered the main reason for this problem [3], to the extent that the discouraged use of bismuth shields has also been warned recently [22].

Hence, the approach to materials with lower atomic numbers (such as aluminium and iron) seems to have attracted much attention in constructing and designing composites. The use of aluminium (Z = 13) in the layout and fabrication of shields in space sciences has a long history [23-24]. On the other hand, the use and exploitation of iron (Z = 26) not only has a much longer history in human life, but also the well-known form of magnetite and the possibility of manufacturing it in tiny dimensions (micro and nano) have shown new capabilities of this element physically and chemically [25]. Magnetite possesses exceptional biocompatibility properties, rendering it an exceptionally efficient contrast agent for applications in magnetic resonance imaging (MRI) [26], hyperthermia [27], and drug delivery [28].

Designing polymer composites by selecting biocompatible polymers, such as polyvinyl alcohol (PVA), can give them new capabilities. Since non-toxic and non-carcinogenic PVA has been approved by the US Food and Drug Administration (FDA), its expedition for food packaging and making some medical biomaterials (such as patella and synthetic cartilage) has turned it into a biocompatible and irreplaceable polymer. However, its other unique properties, such as water solubility, high crystalline degree at low temperatures, optimal mechanical durability, and melting point, can make these capabilities more valuable [29-30].

Despite all the above considerations, few studies have been conducted on this class of polymer composites to design and construct radiation shields. Srinivasan et al. studied the radiation shielding features of composites consisting of PVA/iron oxide in a wide energy range (0.0150 -20.0000 MeV) numerically and found that 50% of magnetite and a similar amount of PVA could provide the highest level of radiation shielding for composite shields compared to pure PVA shields [31]. Hosseini et al. examined the influence of magnetite insertion in several different compositions using the same approach and stated that in the range of low- and medium-energy photons, it could be used as a photon radiation shielding material in medical diagnostic processes along with less secondary radiations [32]. In an experimental study on a new type of composite (polymer blend-Fe3O4) to examine the electrical and optical features, Hashim et al. pointed out the potency of magnetite addition and the improvement of the shielding process against gamma sources [33].

So far, studies on composites containing tungsten and bismuth metals in PVA substrates have reported satisfactory results [7-9]. However, the usefulness of the simultaneous use of heavy and light fillers together (such as bismuth + lighter metal elements) in the design and construction of X-ray and gamma-ray shielding glasses has been confirmed by experimental and computational methods [34-35].

Therefore, given the importance and role of polymer composites in shielding, especially in medical diagnostic and treatment processes, the radiation shielding features of shields consisting of PVA were analyzed in this study in the simultaneous presence of two magnetite and bismuth oxide fillers by different computational methods.

Materials and Methods

Methods for Designing of Composites

This descriptive-analytical study was conducted to investigate composites' shielding features consisting of PVA + magnetite + bismuth oxide against ionizing photon sources. For this purpose, five compounds (B1-B5) were selected according to Table 1 to start the study. In the first three columns of Table 1, the weight distribution of each part of the composite is given, a sample of raw PVA (B5) is considered, and the other four samples (B1, B2, B3, and B4) consist of a constant 30% of the magnetite weight fraction, 10%, 3%, 5%, 7% of bismuth oxide, and the rest accounts for the PVA weight fraction.

In the next columns of Table 1, the distribution of elements in each composition is presented separately. In the last column, the final density of each compound is calculated according to the American Society for Testing and Materials (ASTM) standard [36]

$$\rho_{theorical}\left(\frac{g}{cm^3}\right) = \frac{1}{\left(\frac{W_1}{\rho_1}+\frac{W_2}{\rho_2}+\frac{W_3}{\rho_3}\right)} \quad (1)$$

In Equation 1, W represents the weight fraction of each composite component, and ρ is its corresponding density. In order to calculate the final density for use in the above equation, the densities of PVA, magnetite, and bismuth oxide were considered consistent with the reality and 1.3000, 4.9000, and 8.7000 g/cm^3, respectively.

Then, a rigorous analysis is conducted to explore how five composite materials absorb and attenuate radiation across a wide range of photon energy levels from 0.01000 MeV to 10,000 MeV.

Table 1. The composition of each composite according to the weight distribution of the present elements, along with the mean density of each sample

Sample name	Weight fraction of the compound (wt%)			Weight fraction of the elements (wt%)					ρ(g/cm^3)
	PVA	Fe3O4	Bi2O3	H	C	O	Fe	Bi	
B1	67	30	3	0.0613	0.3653	0.3293	0.21708	0.02691	1.7300
B2	65	30	5	0.0595	0.3544	0.3241	0.2171	0.04485	1.7700
B3	63	30	7	0.0577	0.3435	0.3189	0.2171	0.0628	1.8100
B4	60	30	10	0.0549	0.3272	0.3111	0.2171	0.0897	1.8800
B5	100	0	0	0.0915	0.5453	0.3632	0.00000	0.0000	0.0130

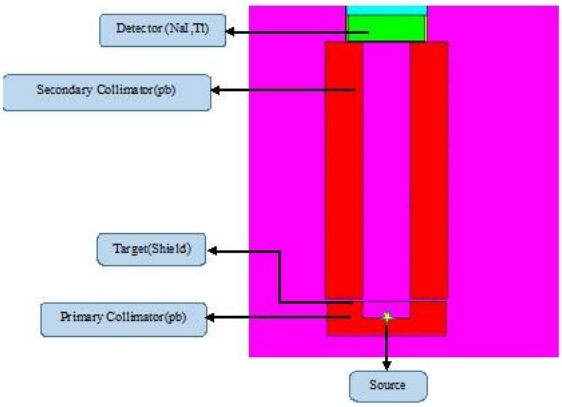

Figure 1. Parallel narrow geometry simulated by the MCNP code for calculating attenuation coefficients in the present study

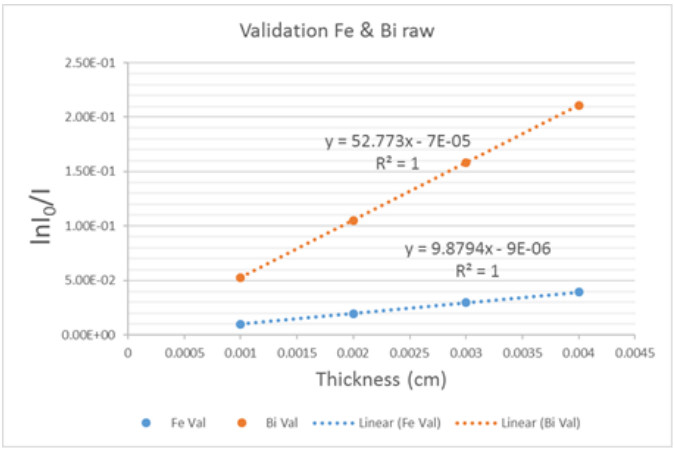

Figure 2. The linear fitting for determination of the linear attenuation coefficient (μ) of bismuth and iron elements

To ensure precision and thoroughness, we calculated essential parameters such as the linear attenuation coefficient (μ), mass attenuation coefficient (μ_ρ), effective atomic number (Z_{eff}), and electron density (N_e). These calculations were carefully performed within specific energy intervals, and the subsequent sections will provide comprehensive details on the methodologies and outcomes.

Calculation of Radiation Factors

The radiation properties of the five composites were extensively evaluated by analyzing several important factors. To estimate the mass attenuation coefficient (μρ), two different techniques (MCNPX and XCOM) were employed. The first one involved using the Monte Carlo N-Particle X (MCNPX) code version 2.6 [37] to simulate photon particle behavior in a setup closely resembling real conditions. The configuration, as shown in Figure 1, involved two lead collimators: one for initial source narrowing (collimator 1) and another for removing scattered radiation (collimator 2). A point source (see Figure 1) emitting photons with a single energy was placed 5 cm deep within the first collimator. A rectangular cube, serving as both a target and shield, was positioned in front of the source with varying thicknesses. The detector, in this geometry, was a cylindrical cell containing sodium iodide with thallium impurities, surrounded by additional cylinders. The geometric efficiency of the detector and material properties can be found in reference [38].

The radiation intensity (I) in this cell was estimated using the F4 Tally calculation, representing particle flux in the detector cell, with 2×10^7 particles specified at program entry (NPS), ensuring a relative error in statistical calculations below 1%. To calculate the mass attenuation coefficient (μρ) parameter in this setup, we calculated the intensities with and without the test material at different thicknesses (X), enabling the use of the Beer-Lambert formula to determine μ [1-2]:

$$I = I_0 e^{-\mu x} \quad (2)$$

The implementation of this formula (Eq.2) is shown in Figure 2. Linear fitting was performed to determine the line slope (equivalent to μ) for validation using iron and bismuth at the selected energy of 0.0590 MeV. By dividing the determined line slope values (μ) by the density of each element (ρ_{Bi} = 9.7490 g/cm^3, ρ_{Fe} = 7.8470 g/cm^3), mass attenuation coefficients (μρ) were obtained. After validating the calculations, the mass attenuation coefficient factor for all five composites was extracted using the same method. The program input utilized the element distribution and density listed in Table 1 to define the target cell material card.

The second method employed to estimate the mass attenuation coefficients relied on accessing the NIST-XCOM database [39]. This database offers the ability to calculate total and partial mass attenuation coefficients for various states (element/compound/mixture). The following formula is used to calculate the mass attenuation coefficient of a composite:

$$\mu_\rho = \frac{\mu}{\rho} = \sum w_i \left(\frac{\mu}{\rho}\right)_i \quad (3)$$

where w_i and $\left(\frac{\mu}{\rho}\right)_i$ represent the weight fraction and mass attenuation coefficient of the i^{th} element in a given composition, respectively. The attenuation coefficients of elements (Z=1-92) were calculated based on datasheets classified by Hubble et al., allowing calculation within the desired energy range (0.0010-10000.0000 MeV here) [40].

Determining key quantities (μ, μρ) in a composite is crucial since they enable the derivation of other important parameters, such as the half-value layer (HVL, the thickness to halve radiation intensity) and the mean free path (mfp, the mean distance between consecutive photon collisions) using the following equations (4, 5):

$$HVL = \frac{\ln 2}{\mu} \quad (4)$$

$$mfp = \frac{1}{\mu} \quad (5)$$

Two additional fundamental parameters utilized in this study for enhanced radiation analysis of composites were Z_{eff} (effective atomic number) and N_e (number of electrons in mass). These parameters have significant implications in medical radiation dosimetry for tasks like calculating radiation dose in radiotherapy and CT scans [41-42]. However, Z_{eff} and N_e are energy-dependent when viewed in the context of photon energy, making them valuable for understanding processes within materials, such as changes in the photoelectric effect, Compton scattering, and pair production. This radiation analysis method in materials has applications in diverse fields, including biological environments [41], composites, and radiation shields [32, 42-45].

To calculate Z_{eff}, we employed dedicated software called Auto-Zeff, previously developed and reported in 1998 [46]. However, a direct method also exists, allowing the calculation of Z_{eff} through updated specific formulas. Since both methods rely on the energy-dependent mass attenuation coefficient, using updated data to determine this quantity more accurately through the second method is logical. To calculate Z_{eff} via the direct method, we first calculated two factors: atomic cross-section level (σ_a) and electron (σ_e) using the following equations:

$$\sigma_a = \frac{\mu_m}{N_A \sum_i \frac{w_i}{A_i}} \quad (6)$$

where N_A represents Avogadro's constant, and A_i represents the atomic weight of the i^{th} element in cm^2/atom. The electronic cross-section was calculated using this formula:

$$\sigma_e = \frac{1}{N_A} \sum_i \left(\frac{\mu}{\rho}\right)_i \frac{f_i A_i}{Z_i} \quad (7)$$

where Z_i and f_i are the atomic number and fraction frequency of the i^{th} element, respectively, with units in cm^2/electron. Finally, Z_{eff} was calculated by dividing σ_a by σ_e:

$$Z_{eff} = \frac{\sigma_a}{\sigma_e} \quad (8)$$

Another important parameter, N_e, representing the number of electrons per mass unit, can be calculated after determining Z_{eff}:

$$N_e = N_A \frac{Z_{eff}}{\sum_i f_i A_i} \quad (9)$$

In the above equation, N_e is expressed in electrons per gram. The total mass attenuation coefficients required to calculate Z_{eff} and N_e for the five composites were computed using calculations and data extraction from the NIST-XCOM database [39].

Results

In this study, we investigated iron and bismuth properties at 0.0590 MeV energy, calculating their mass attenuation coefficients. Using MCNP, we found coefficients of 1.2550 cm²/g for iron and 5.4140 cm²/g for bismuth, closely matching reference values from NIST-XCOM (1.2590 cm²/g for iron and 5.4630 cm²/g for bismuth). The difference was less than 0.1%, affirming method accuracy and geometry design validation.

Based on the accuracy of the primary calculations, the trend of changes in mass attenuation coefficients regarding energy for the five studied compounds in Figure 3 can now be comprehendible, where the values calculated through XCOM are shown as a continuous line, and the results extracted from the MCNP code at several energies are represented through dots.

Also, for better understanding, the values of mass attenuation coefficients in selected energy (0.0590 MeV) are given in Table 2 regarding both methods. The

computational deviation rate (MCNP relative to XCOM) is also calculated in the last column of this table.

A glance at Figure 3 shows that matching the two methods in other selective energies (matching of line and discrete points) is seen in all cases, and this consistency is also seen in the last column of Table 2, where the maximum difference in values between the two methods does not exceed 1%.

The process of mass attenuation alters for the five composites can be outlined as follows: at low-energy ranges (E < 0.1500 MeV), the effect of adding fillers is well visible; thus, with the gradual addition of fillers to the raw sample (B5), a significant increase is observed in mass attenuation curves. In this area, sudden rises in the form of sharp energy peaks are apparent in the diagram, and the fingerprints of bismuth are thoroughly visible in some energies, such as 0.0026, 0.0027, 0.0032, 0.0037, 0.0040, 0.0134, 0.0157, 0.1640, 0.0905 MeV, belonging to the recognized edges (K, L, M) [39]. Furthermore, the K-edge energy peak belonging to iron (at 0.0071-MeV energy) manifested in the same range of energy, which at energies corresponding to these edges, a significant surge in the photoelectric effect is expected. A negligible and inconsiderable effect can be seen in the next energy range by adding fillers to the composites. In other words, with the addition of the filler, no superiority was observed in the mass attenuation coefficient. It is noteworthy that composites with fillers exhibit increasing curves above 10.0000 MeV, as illustrated in Figure 3.

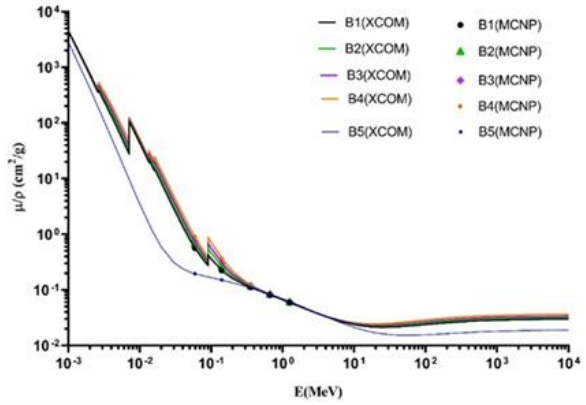

Figure 3. The trend of changes of total mass attenuation coefficients for B1-B5 composites in a wide energy range by MCNP and XCOM methods

Table 2. The values of mass attenuation coefficients obtained for the five composites studied through XCOM and MCNP methods at the 0.059 MeV selected energy extracted from Figure 3

Sample name	μ_ρ(cm^2/gr) MCNP	μ_ρ(cm^2/gr) XCOM	Relative error%
B1	0.5634	0.5681	0.8240
B2	0.6598	0.6626	0.4240
B3	0.7520	0.7571	0.6760
B4	0.8941	0.8988	0.5230
B5	0.1953	0.1959	0.3020

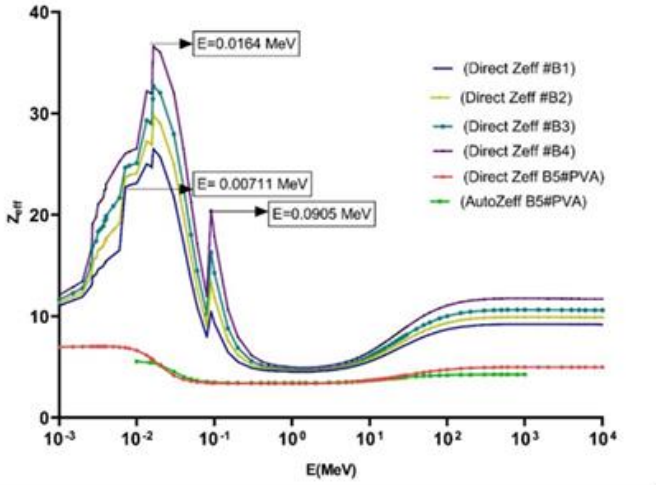

Figure 4. The trend of changes in atomic number values in terms of energy for the five studied composites.

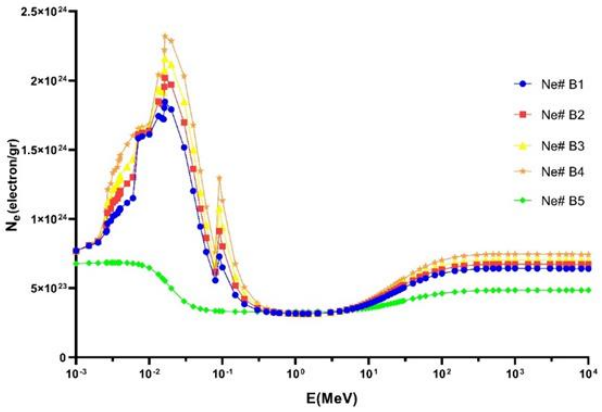

Figure 5. The estimated values of electron per gram unit in terms of energy for the five studied composites.

The trend of Z_{eff} changes in Figure 4 and N_e in Figure 5 at similar energy ranges (Figure 3) are shown here. The accuracy of Zeff's calculations, the consequential quantity, is shown in Figure 4, where Z_{eff}'s results are illustrated, for example, B5 with good consistency with both direct and Auto-Z methods. A simultaneous review of the Z_{eff} (Figure 4) and N_e (Figure 5) belonging to the five composites includes several distinguished points to better illustrate the radiation attenuation and absorption process. As seen in the filler-free sample (B5), the atomic number and N_e have the lowest values. However, in samples containing fillers of bismuth and iron elements, by increasing bismuth concentration, the values of the Z_{eff} and N_e showed a significant increase. For example, the trend of changes in Z_{eff} values among filler-containing composites, with the lowest (B1) and highest (B4) concentrations of bismuth oxide, reached from 22 to 26 at 0.0071 MeV, from 26 to 37 at 0.0164 MeV, and from 10 to 20 at 0.0905 MeV.

The assessment of the trend of atomic number variations in terms of energy in composites showed that at low energies (approximately less than 0.0160 MeV), the Z_{eff} significantly increased; thus, the highest Z_{eff} value of 36.6000 in the B4 composite (containing the highest concentration of bismuth filler) is shown in the diagram. Similarly, instant surges in some of the lower energies are illustrated in the diagram. Accordingly, it is clearly distinguishable how the energy absorption edges played an important role in increasing the Z_{eff}. On the other hand, the increase in the Z_{eff} in this region can be attributed to the dominance of the photoelectric effect over another possible phenomenon (Compton). Therefore, this range can be called the absorption region [43-44].

As illustrated, with increasing energy in the next range ($0.0160 < E < 0.0905$ MeV), a declining trend in the Z_{eff} is observed, and with approaching the next adsorption edge of bismuth (Ek = 0.0905 MeV), the reversal trend accompanies an increase in the Z_{eff}, and then a reduction is observed again (up to an energy of less than 0.3560 MeV). The reason for the decline in the Z_{eff} (after undergoing a reversal trend) was related to the reduction of the photoelectric and its substitution with the Compton effect [43-44]. The radiation attenuation is estimated in this energy region.

By tracking energy in both diagrams, the Z_{eff} and N_e formed the plateau region, and this trend appears to have continued at energies less than 3 MeV. In explaining this trend, the dominance of the Compton effect ($E < 1.2200$ MeV) and the subsequent formation of the pair production effect were cited as reasons for observing this trend. Therefore, high distribution in this region is predictable. However, in the region of higher energies, energy dependence in the values of the Z_{eff} and N_e was observed again along with the increasing trend. The cause can be attributed to the dominance of the pair production effect [43-44].

The data in Table 3 shows the values of μ, HVL thickness, and mfp at various photopeak energies for commonly used radioactive sources. These sources include Am-241 (0.0590MeV), Tc-99m (0.1400MeV), Ba-133 (0.3560MeV), Cs-137 (0.6620MeV), and Co-60 (1.2500MeV), which are suitable for a range of medical diagnosis and treatment studies [6-8, 32]. The data was obtained using MCNP and XCOM methods.

It was observed that the attenuation and absorption processes improved by increasing the concentration of fillers. This point can be confirmed by the HVL-reduced value in each of the specific energies. For example, at 0.0590-MeV energy (which is in the range of the mean radiation energy in most CT scan devices), the desired improvement in the attenuation process can be found by decreasing the HVL values from 2.7300 cm to 0.4100 cm in the MCNP code (very similar to XCOM). The reason for this issue may be better explained by referring to mfp values. In other words, as is obvious in the mentioned energy, mfp values in the samples containing the lowest and highest amounts of fillers decreased from 3.9400 cm to 0.6000 cm. It means that in the presence of fillers with a higher weight percentage of bismuth oxide, the distance between the two consecutive photon collisions is reduced, diminishing the thickness required to halve the HVL radiation intensity. Also, evaluating the trend of changes in the values of Table 3 shows that with increasing the given energies, attenuation; and absorption decrease, and with increasing photon energy and its higher penetration depth in composite materials, HVL also increases.

Table 3. Estimating the linear attenuation coefficient quantities, HVL thickness, and mfp for the studied composites in several selected energies by MCNP and XCOM code methods

E(MeV)	Sample	MCNP			XCOM		
		μ(cm^{-1})	HVL(cm)	mfp(cm)	μ (cm^{-1})	HVL(cm)	mfp(cm)
0.0590	B1	0.9700	0.7100	1.0300	0.9800	0.7100	1.0200
	B2	1.1700	0.5900	0.8600	1.1700	0.5900	0.8500
	B3	1.3600	0.5100	0.7300	1.3700	0.5100	0.7300
	B4	1.6800	0.4100	0.6000	1.6900	0.4100	0.5900
	B5	0.2500	2.7300	3.9400	0.2500	2.7200	3.9300
0.1400	B1	0.3900	1.7900	2.5800	0.3900	1.7800	2.5600
	B2	0.4700	1.4900	2.1500	0.4700	1.4700	2.1200
	B3	0.5500	1.0100	1.4600	0.5600	1.2400	1.7900
	B4	0.6900	1.0100	1.4600	0.7000	0.9900	1.4300
	B5	0.2000	3.5300	5.0900	0.2000	3.5500	5.1200
0.3560	B1	0.1900	3.6000	5.1900	0.1900	3.6000	5.2000
	B2	0.2000	3.3900	4.8900	0.2000	3.4200	4.9400
	B3	0.2100	3.2500	4.6900	0.2100	3.2400	4.6800
	B4	0.2300	3.0100	4.3500	0.2300	3.0000	4.3300
	B5	0.1400	4.9400	7.1200	0.1400	4.8900	7.0600
0.6620	B1	0.1400	4.8900	7.0600	0.1400	4.8900	7.0600
	B2	0.1500	4.7600	6.8600	0.1500	4.7500	6.8600
	B3	0.1500	4.6200	6.6700	0.1500	4.6100	6.6600
	B4	0.1600	4.4200	6.3700	0.1600	4.4100	6.3600
	B5	0.1100	6.3200	9.1200	0.1100	6.34000	9.1400
1.2500	B1	0.1000	6.7000	9.6700	0.1000	6.7200	9.7000
	B2	0.1100	6.5600	9.4700	0.1100	6.5700	9.4800
	B3	0.1100	6.3900	9.2200	0.1100	6.4300	9.2700
	B4	0.1100	6.2300	8.9900	0.1100	6.2100	8.9500
	B5	0.0800	8.6000	12.4100	0.0800	8.5900	12.4000

Discussion

Five different composites made of PVA, magnetite, and bismuth oxide were analyzed in this study. Numerical calculation and modeling methods were utilized in the MCNP code, along with data from the NIST-XCOM database, to evaluate their protective capabilities across a broad range of energies (0.0010-10000.0000 MeV). It appears necessary to mention a few points here:

The first point underscores the crucial selection of magnetite and bismuth oxide fillers in this study, emphasizing magnetite's unique properties and well-documented biocompatibility [25-28]. Despite the use of magnetite in shielding non-ionizing electromagnetic waves [47-49], it seems that the use of magnetite properties in constructing and designing radiation shielding materials (especially photon ionizing radiations) is at the beginning of the road and has been seen in only a few studies [31-33]. Instead, applying bismuth oxide in the design and construction of polymer composites, along with its special efficiency in absorbing low- and medium-energy ionizing photons, has been reported in previous studies [5-6]. Despite the specific and clinical use of bismuth in shielding superficial and radiation-sensitive tissues in diagnostic processes, especially their long history in CT scans, its efficiency has been seriously challenged in many studies due to the imbalance between reducing the dose in the patient and the image quality [17, 19-21], and even the discouragement to use it has been raised [22]. The main reason for this challenge may be related to the overproduction of secondary radiation after collisions, which reduces image quality. Therefore, the approach to materials with low atomic numbers (Low-Z) may be a basic solution to further alleviate secondary radiation [3, 32]. Recent investigations have delved into the substitution of bismuth with lower atomic number materials, such as copper, yielding promising outcomes [50-51].

The second point here is related to the usefulness, though few, of low atomic number fillers such as magnetite.

Srinivasan et al. numerically studied the use of magnetite in PVL in the presence of photon sources equal to the energies used in CT scans [31]. Hosseini et al. also examined numerous compounds of magnetite/polyethylene and demonstrated its efficiency in diagnostic processes in radiology and nuclear medicine [32].

The third point, as seen in this study, was that the addition of magnetite fillers (with a constant weight percentage of 30%), along with bismuth oxide (with different percentages, 3%, 5%, 7%, and 10%) to the matrix (PVA), could lead to a significant increase in the radiation attenuation and absorption process. This

superiority was well seen up to medium energies (E ~ 356.0000 keV). This point was observed by examining the trend of mass attenuation coefficients (Figure 3), along with the emergence of sharp energy peaks (increase in absorption at low energies [E < 0.1000 MeV]), which were consistent with the edges of energy absorption feature of bismuth and iron elements. Assessing the trend of alterations in the Zeff and Ne respecting energy (Figures 4 and 5) first showed a similar trend of changes and is consistent with previous studies [43-44]. In the mentioned studies, also, similar methods were used to describe the behavior of materials in the presence of radiation (the study of the photoelectric effect, Compton effect, and even pair production).

The results of this study showed that at low energies (E < 0.1000 MeV), the increase and dominance of the photoelectric effect led to more absorption, and in the next range (0.1000 < E < 0.3560 MeV), the Compton effect was substituted with the photoelectric effect. The increased probability of the Compton effect can lead to absorption and attenuation. However, at higher energies (E >0.3560 MeV), scattering is predicted due to the dominance of the Compton effect (observing the plateau and energy-independent region in the curves in Figure 4), and finally (E > 1.2200MeV), the emergence and subsequent dominance of the pair production effect in filler-containing composites (B1-B4) are well predicted.

Finally, a numerical analysis, μ quantities, HVL, and mfp at five selected energies of 0.0590, 0.1400, 0.3560, 0.6110, 1.2500 MeV demonstrated an improved radiation absorption process by increasing the weight concentrations of the bismuth oxide filler, which was remarkable compared to the raw sample (B5). However, with increasing energy (as a result of more photon permeability) in samples (B1-B4), as expected, a diminishing trend in photon absorption was observed. The trend of alterations in mfp values and its dependence on the material type (μ) and photon energy (E) in all composites (B1-B5) are well consistent with the principles cited in references [1, 2].

Considering all the above-mentioned points, the method used in this research aimed to reduce bismuth (as a high atomic number, Z = 83) and substitute a part of it with magnetite (with a lower atomic number, Z = 26), and PVA (as a biopolymer compatible with a low atomic number), may be considered a novel approach to address the needs and overcome the present challenges in radiation shields. Since the investigated mean energy range (0.0500-0.0800 MeV) is applied in multi-detector CT scan (MDCT) and dual-energy CT scan devices which correspond to 80.0000 to 140.0000 kVp [52] and, on the other hand, a desirable behaviour was observed in radiation absorption and attenuation, the continuation of this study can be well justified on operational phases.

Conclusion

The attenuation and absorption of ionizing photon radiation in five composites with varying weight fractions of PVA, magnetite, and bismuth oxide were estimated and analyzed. This was achieved through modeling and calculations utilizing the Monte Carlo simulation code and XCOM.

In the presence of the mentioned fillers (magnetite/bismuth oxide), considerable radiation absorption and attenuation were observed compared to the filler-free sample (raw PVA). However, with increasing the amount of the bismuth oxide filler, these superiorities were observed in the graphs of mass attenuation coefficients up to the medium energies. In confirming these observations, the trend of changes in the Zeff and Ne in different energy ranges showed increased absorption due to the dominance of the photoelectric effect in the low-energy region (<0.1000 MeV), attenuation due to substitution, and the increasing trend of the Compton effect (0.1000 < E < 0.3560 MeV), and scattering at higher energies (E > 0.3560 MeV), is first due to the dominance of the Compton effect, and finally, the emergence and dominance of the pair production effect (E > 1.2200 MeV). This superiority was also seen by the quantitative analysis of the HVL, MFP, and μ at several selected energies (0.0590, 0.1400, 0.3560, 0.6110, 1.2500 MeV); thus, by increasing the concentration of the bismuth oxide filler, the HVLs decreased to a desirable amount; however, for each given composite, this amount increased as the energy increased.

The importance of the composites studied in this research can be summarized as follows: First, introducing new lead-free compounds to meet the challenges of lead (such as toxicity and high weight of products) with desirable efficiencies at the same time in the range of low and medium energies of ionizing photons.

The second fact that should not be overlooked is the possibility of reducing bismuth as much as possible and substituting it with materials with lower atomic numbers, such as magnetite and PVA. The method used in this study is expected to culminate in less secondary radiation than pure bismuth. This issue can be considered especially in designing the shielding materials of superficial and sensitive tissues in radiological diagnostic processes (especially CT scans) and designing aprons. Therefore, according to the promising results of this study, researchers strongly recommend further studies and the beginning of the practical phase of construction and experimental studies of the shielding features of these composites.

Acknowledgment

This article is an excerpt from an MSc thesis by Fariba Baroonzadeh, sponsored by the Research Deputy of Shiraz University of Medical Sciences (project No 23145), and it was also approved by the Ethics Committee of Shiraz University of Medical Sciences under the code IR.SUMS.REC.1400.291.

References

1. Cember H, Johnson T. Introduction to Health Physics. 4th ed., McGraw-Hill Medical: New York; 2009.
2. Chilton AB, Shultis JK, Faw RE. Principles of radiation shielding. Englewood Cliffs, NJ: Prentice Hall; 1984.
3. Nambiar S, Yeow JT. Polymer-composite materials for radiation protection. ACS Appl Mater Interfaces. 2012 Nov 28;4(11):5717-26.
4. More CV, Alsayed Z, Badawi M, Thabet A, Pawar PP. Polymeric composite materials for radiation shielding: a review. Environ Chem Lett. 2021 Aug 1;19(3):2057-90.
5. Ambika MR, Nagaiah N, Suman SK. Role of bismuth oxide as a reinforcer on gamma shielding ability of unsaturated polyester based polymer composites. J Appl Polym Sci. 2017 Jul 1;134(13):44657.
6. Mehrara R, Malekie S, Kotahi SM, Kashian S. Introducing a novel low energy gamma ray shield utilizing polycarbonate bismuth oxide composite. Sci Rep. 2021 Jan 12;11(1):1-3.
7. Hosseini MA, Malekie S, Kazemi F. Experimental evaluation of gamma radiation shielding characteristics of polyvinyl alcohol/tungsten oxide composite: A comparison study of micro and nano sizes of the fillers. Nucl Instrum Methods Phys Res A. 2022 Feb;1026:166214.
8. Hosseini MA, Kazemi F, Malekie S. A Monte Carlo study on the shielding properties of a novel polyvinyl alcohol (PVA)/WO3 composite, against gamma rays, using the MCNPX code. J Biomed Phys Eng. 2019 Dec;9(4):465.
9. Noor Azman NZ, Musa NF, Nik Ab Razak NN, Ramli RM, Mustafa IS, Abdul Rahman A, et al. Effect of Bi2O3 particle sizes and addition of starch into Bi2O3–PVA composites for X-ray shielding. Appl Phys A. 2016 Sep;122(9):1-9.
10. Brenner DJ, Hall EJ. Computed tomography—an increasing source of radiation exposure. N Engl J Med. 2007 Nov 29;357(22):2277-84.
11. Mathews JD, Forsythe AV, Brady Z, Butler MW, Goergen SK, Byrnes GB, et al. Cancer risk in 680,000 people exposed to computed tomography scans in childhood or adolescence: data linkage study of 11 million Australians. BMJ. 2013 Mar 12;346:f2360.
12. Dellie ST, Tesfaw AF. Evaluation of Local Diagnostic Reference Levels for Paediatric and Adult Patients Undergoing Head Computed Tomography Examination in Amhara Regional States, Ethiopia. Iran J Med Phys. 2023 Sep 1;20(5).
13. Abyar M, Mahdavi M, Haddadi GH. Establishing local Diagnostic Reference Level for Adult Patients in Computed Tomography Examination in Kohgiluyeh and Boyer-Ahmad province. Iran J Med Phys. 2021 Jul 1;18(4).
14. Okoro NO, Changizi V, Bagh EJ, Pak F. Optimization of Radiation Dose in Cranial Computed Tomography among Adults: Assessment of Radiation Dose against Image Quality. Iran J Med Phys. 2020 Sep 1;17(5).
15. Asadinezhad M, Bahreyni Toossi MT, Nouri M. Diagnostic reference levels for computed tomography examinations in Iran: a nationwide radiation dose survey. Iran J Med Phys. 2019 Jan 1;16(1):20.
16. Bahreyni Toossi MT, Zare H, Eslami Z, Bayani Roodi S, Daneshdoust M, Saeed Z, et al. Assessment of Radiation Dose to the Lens of the Eye and Thyroid of Patients Undergoing Head and Neck Computed Tomography at Five Hospitals in Mashhad, Iran. Iran J Med Phys. 2018 Oct 1;15(4):226-30.
17. Mehnati P, Malekzadeh R, Sooteh MY. Use of bismuth shield for protection of superficial radiosensitive organs in patients undergoing computed tomography: a literature review and meta-analysis. Radiol Phys Technol. 2019 Mar;12(1):6-25
18. Okoro NO, Changizi V, Bagh EJ, Pak F. Optimization of Radiation Dose in Cranial Computed Tomography among Adults: Assessment of Radiation Dose against Image Quality. Iran J Med Phys. 2020 Sep 1;17(5).
19. Kawauchi S, Chida K, Moritake T, Hamada Y, Tsuruta W. Radioprotection of eye lens using protective material in neuro cone-beam computed tomography: Estimation of dose reduction rate and image quality. Phys Med. 2021 Apr;82:192-9.
20. Kim MS, Choi J, Kim SY, Kweon DC. Adaptive statistical iterative reconstruction and bismuth shielding for evaluation of dose reduction to the eye and image quality during head CT. J Korean Phys Soc. 2014 Jun;64(6):923-8.
21. Einstein AJ, Elliston CD, Groves DW, Cheng B, Wolff SD, Pearson GD, et al. Effect of bismuth breast shielding on radiation dose and image quality in coronary CT angiography. J Nucl Cardiol. 2012 Feb;19(1):100-8.
22. McCollough CH, Wang J, Gould RG, Orton CG. The use of bismuth breast shields for CT should be discouraged. Med Phys. 2012 May;39(5):2321-4.
23. Durante M. Space radiation protection: destination Mars. Life Sci Space Res. 2014;1:2-9.
24. Daneshvar H, Milan KG, Sadr A, Sedighy SH, Malekie S, Mosayebi A. Multilayer radiation shield for satellite electronic components protection. Sci Rep. 2021 Jan 8;11(1):1-2.
25. Sun J, Zhou S, Hou P, Yang Y, Weng J, Li X, et al. Synthesis and characterization of biocompatible Fe3O4 nanoparticles. J Biomed Mater Res A. 2007 Feb;80(2):333-41.
26. Arsalani N, Fattahi H, Nazarpoor M. Synthesis and characterization of PVP-functionalized superparamagnetic Fe3O4 nanoparticles as an MRI contrast agent. Express Polym Lett. 2010 Jun;4(6):329-38.
27. Oltolina F, Peigneux A, Colangelo D, Clemente N, D'Urso A, Valente G, et al. Biomimetic magnetite nanoparticles as targeted drug nanocarriers and mediators of hyperthermia in an experimental cancer model. Cancers. 2020 Sep 4;12(9):2564.
28. Yew YP, Shameli K, Miyake M, Khairudin NB, Mohamad SE, Naiki T, et al. Biosynthesis of superparamagnetic magnetite Fe3O4 nanoparticles and biomedical applications in targeted anticancer drug delivery system: A review. Arab J Chem. 2020 Jan;13(1):2287-308.
29. DeMerlis CC, Schoneker DR. Review of the oral toxicity of polyvinyl alcohol (PVA). Food Chem Toxicol. 2003 Mar;41(3):319-26.

30. Baker MI, Walsh SP, Schwartz Z, Boyan BD. A review of polyvinyl alcohol and its uses in cartilage and orthopedic applications. J Biomed Mater Res Part B. 2012 Oct;100B(6):1451-7.
31. Srinivasan K, Samuel EJ. Evaluation of radiation shielding properties of the polyvinyl alcohol/iron oxide polymer composite. J Med Phys. 2017 Oct-Dec;42(4):273.
32. Hosseini M, Malekie S, Keshavarzi M. Analysis of radiation shielding characteristics of magnetite/high density polyethylene nanocomposite at diagnostic level using the MCNPX, XCOM, XMudat and Auto-Zeff programs. Mosc Univ Phys. 2021;76(Suppl 1):S52-61.
33. Hashim A, Agool IR, Kadhim KJ. Novel of (polymer blend-Fe3O4) magnetic nanocomposites: preparation and characterization for thermal energy storage and release, gamma ray shielding, antibacterial activity and humidity sensors applications. J Mater Sci: Mater Electron. 2018 Jun;29(12):10369-94.
34. Issa SA, Ahmad M, Tekin HO, Saddeek YB, Sayyed MI. Effect of Bi2O3 content on mechanical and nuclear radiation shielding properties of Bi2O3-MoO3-B2O3-SiO2-Na2O-Fe2O3 glass system. Results Phys. 2019 Jun 1;13:102165.
35. Elmahroug Y, Almatari M, Sayyed MI, Dong MG, Tekin HO. Investigation of radiation shielding properties for Bi2O3-V2O5-TeO2 glass system using MCNP5 code. J Non Cryst Solids. 2018 Jul;499:32-40.
36. ASTM Committee D-20 on Plastics. Standard test methods for density and specific gravity (relative density) of plastics by displacement. ASTM D20.70.01. American Society for Testing and Materials.
37. Pellowitz D. MCNPX User′s Manual, version 2.6.0. Los Alamos Report No. LA CP. 2007; 2:408.
38. Tekin HO. MCNP-X Monte Carlo code application for mass attenuation coefficients of concrete at different energies by modeling 3×3 inch NaI(Tl) detector and comparison with XCOM and Monte Carlo data. Sci Technol Nucl Install. 2016 Dec 1; 2016:334-40.
39. NIST XCOM. Element/compound/mixture—physical measurement. National Institute of Standards and Technology. Available from: https://physics.nist.gov/PhysRefData/Xcom/Text/ref.html. Accessed Nov 2024.
40. Hubbell J. Photon cross sections, attenuation coefficients and energy absorption coefficients. Natl Bur Stand (US) Rep No. NSRDS-NBS29, Washington DC. 1969 Aug.
41. Manohara SR, Hanagodimath SM, Gerward L. Energy dependence of effective atomic numbers for photon energy absorption and photon interaction: studies of some biological molecules in the energy range 1 keV–20 MeV. Med Phys. 2008 Jan;35(1):388-402.
42. Manohara SR, Hanagodimath SM, Thind KS, Gerward L. On the effective atomic number and electron density: a comprehensive set of formulas for all types of materials and energies above 1 keV. Nucl Instrum Methods Phys Res B. 2008 Oct;266(18):3906-12.
43. Büyükyıldız M. Effective atomic numbers and electron densities for some lanthanide oxide compounds using direct method in the energy region of 1 keV-20 MeV. Bitlis Eren Univ J Sci Technol. 2016 Jan 1;6(1):7-12.
44. Akyildirim H. Attenuation parameters and effective atomic numbers of concretes containing pumice for some photon energies by experiment, simulation and calculation. Avr Sci Technol J. 2018;14:90-5.
45. Kucuk N, Cakir M, Isitman NA. Mass attenuation coefficients, effective atomic numbers and effective electron densities for some polymers. Radiat Prot Dosim. 2013 Jan 1;153(1):127-34.
46. Taylor ML, Smith RL, Dossing F, Franich RD. Robust calculation of effective atomic numbers: The Auto-Zeff software. Med Phys. 2012 Apr;39(4):1769-78.
47. Olad A, Shakoori S. Electromagnetic interference attenuation and shielding effect of quaternary Epoxy-PPy/Fe3O4-ZnO nanocomposite as a broadband microwave-absorber. J Magn Magn Mater. 2018 Jul 15;458:335-45.
48. Chen Y, Wang Y, Zhang HB, Li X, Gui CX, Yu ZZ. Enhanced electromagnetic interference shielding efficiency of polystyrene/graphene composites with magnetic Fe3O4 nanoparticles. Carbon. 2015 Feb 1;82:67-76.
49. Huangfu Y, Liang C, Han Y, Qiu H, Song P, Wang L, et al. Fabrication and investigation on the Fe3O4/thermally annealed graphene aerogel/epoxy electromagnetic interference shielding nanocomposites. Compos Sci Technol. 2019 Jan 5;169:70-5.
50. Saba V, Keshtkar M. Targeted radiation energy modulation using Saba shielding reduces breast dose without degrading image quality during thoracic CT examinations. Physica Medica. 2019 Sep 1;65:238-46.
51. Keshtkar M, Blouri B, Mahmoudabadi A, Alami A. Eye radiation dose saving in head CT examinations using copper-bismuth radiation shield. Radiat Prot Dosimetry. 2023 Feb;199(2):146-51.
52. Van Elmpt W, Landry G, Das M, Verhaegen F. Dual energy CT in radiotherapy: current applications and future outlook. Radiother Oncol. 2016 Apr 1;119(1):137-44.